Journal of Alloys and Compounds 509 (2011) 2993–2999

Contents lists available at ScienceDirect

Journal of Alloys and Compounds

journal homepage: www.elsevier.com/locate/jallcom

Phase evolution, crystal structure and dielectric behavior of $(1-x)\mathrm{Nd}(\mathrm{Zn}_{0.5}\mathrm{Ti}_{0.5})\mathrm{O}_3 + x\mathrm{Bi}(\mathrm{Zn}_{0.5}\mathrm{Ti}_{0.5})\mathrm{O}_3$ compound ceramics

Mingzhe Hu[a,*], Chunya Luo[a], Huyong Tian[a,b], Haoshuang Gu[a]

[a] Faculty of Electronic Sci&Tech, Hubei University, Xueyuan Road 11, Wuchang District, Wuhan, Hubei 430062, PR China
[b] Dept. of Imaging and Applied Physics, Curtin University of Technology, GPO Box U 1987, Perth, 6845, WA, Australia

ARTICLE INFO

Article history:
Received 25 June 2010
Received in revised form
11 November 2010
Accepted 15 November 2010
Available online 4 December 2010

Keywords:
Complex perovskites
Microwave dielectrics
Radio frequency
Long range ordering structure
Octahedral tilting structure
Temperature compensation

ABSTRACT

The phase evolution, crystal structure and dielectric properties of $(1-x)\mathrm{Nd}(\mathrm{Zn}_{0.5}\mathrm{Ti}_{0.5})\mathrm{O}_3 + x\mathrm{Bi}(\mathrm{Zn}_{0.5}\mathrm{Ti}_{0.5})\mathrm{O}_3$ compound ceramics ($0 \le x \le 1.0$, abbreviated as $(1-x)$NZT–xBZT hereafter) were investigated. A pure perovskite phase was formed in the composition range of $0 \le x \le 0.05$. The B-site $\mathrm{Zn}^{2+}/\mathrm{Ti}^{4+}$ 1:1 long range ordering (LRO) structure was detected by both XRD and Raman spectra in $x \le 0.05$ samples. However, this LRO structure became gradually degraded with an increase in x. The dielectric behaviors of the compound ceramic at various frequencies were investigated and correlated to its chemical composition and crystal structure. A gradually compensated τ_f value was obtained in $(1-x)$NZT–xBZT microwave dielectrics at $x = 0.03$, which was mainly due to the dilution of dielectric constant in terms of Claussius–Mossotti differential equation.

1. Introduction

Complex perovskites with the formula $\mathrm{Ln(M,Ti)O_3}$ (Ln = La, Nd; M = Mg, Co, Zn) have been found to possess extremely high *Qf* value in microwave frequencies, which is suitable for frequency selectivity in satellite communication [1–5]. From a structural viewpoint, these complex perovskites crystallized in monoclinic $P2_1/n$ space group, where a long range B-site ordering structure was permitted to coexist with tilted oxygen octahedra in the perovskite network. The former was generally thought to be one of the most important origins for the ultrahigh *Qf* values in these complex perovskites [2,6,7]. While the latter made these ceramics feature large negative temperature coefficients [7,8] and precluded their practical utilizations in industry. One way out of this dilemma was to form a solid solution with another positive temperature coefficient compound to stretch the tilted oxygen octahedra and compensate the negative τ_f value. For example, $\mathrm{CaTiO_3}$, a typical incipient ferroelectric dielectric with large positive temperature coefficient of ∼+800 ppm/°C, has been employed to form solid solutions with many complex perovskites and successfully tuned their negative τ_f values to near zero [1,9–11].

It is well known that bismuth(III) based dielectric ceramics also feature ferroelectric properties because of the large polarizability of Bi^{3+} cation in perovskites [12]. This character can positively increase τ_f value and relative permittivity in dielectrics. Moreover, owing to the low melting point of $\mathrm{Bi_2O_3}$ component [13], it can also serve as a sintering aid to lower the sintering temperature while improve the sinterability of bismuth(III) containing ceramics. For example, $\mathrm{Bi(Mg_{1/2}Ti_{1/2})O_3}$ compound has been used as a virtual end member in $\mathrm{La(Mg_{1/2}Ti_{1/2})O_3}$ system to improve the dielectric responses and lower the sintering temperature from 1550 °C to 1200 °C [14]. In the present article, Bi^{3+} cation was also employed to modify the dielectric properties as well as sintering behaviors of $\mathrm{Nd(Zn_{1/2}Ti_{1/2})O_3}$ (NZT) ceramic. It was reported that NZT ceramic possessed a significant high *Qf* value of 40,000 GHz and a negative τ_f value of −49 ppm/°C [10,15]. With the substitution of higher polarizability Bi^{3+} for A-site Nd^{3+}, it was anticipated that a compensated τ_f value and an increased relative permittivity in $(1-x)$NZT–xBZT system would be obtained. The microstructure, crystal structure and dielectric behaviors, especially the relationship between the crystal structure and the temperature coefficient in $(1-x)$NZT–xBZT complex perovskites, were thoroughly investigated in order to reveal

---

[*] Corresponding author. Fax: +86 027 8662550.
E-mail addresses: mzhu74@hubu.edu.cn, mingzhe-hu@163.com (M. Hu).

0925-8388/$ – see front matter © 2010 Elsevier B.V. All rights reserved.
doi:10.1016/j.jallcom.2010.11.181

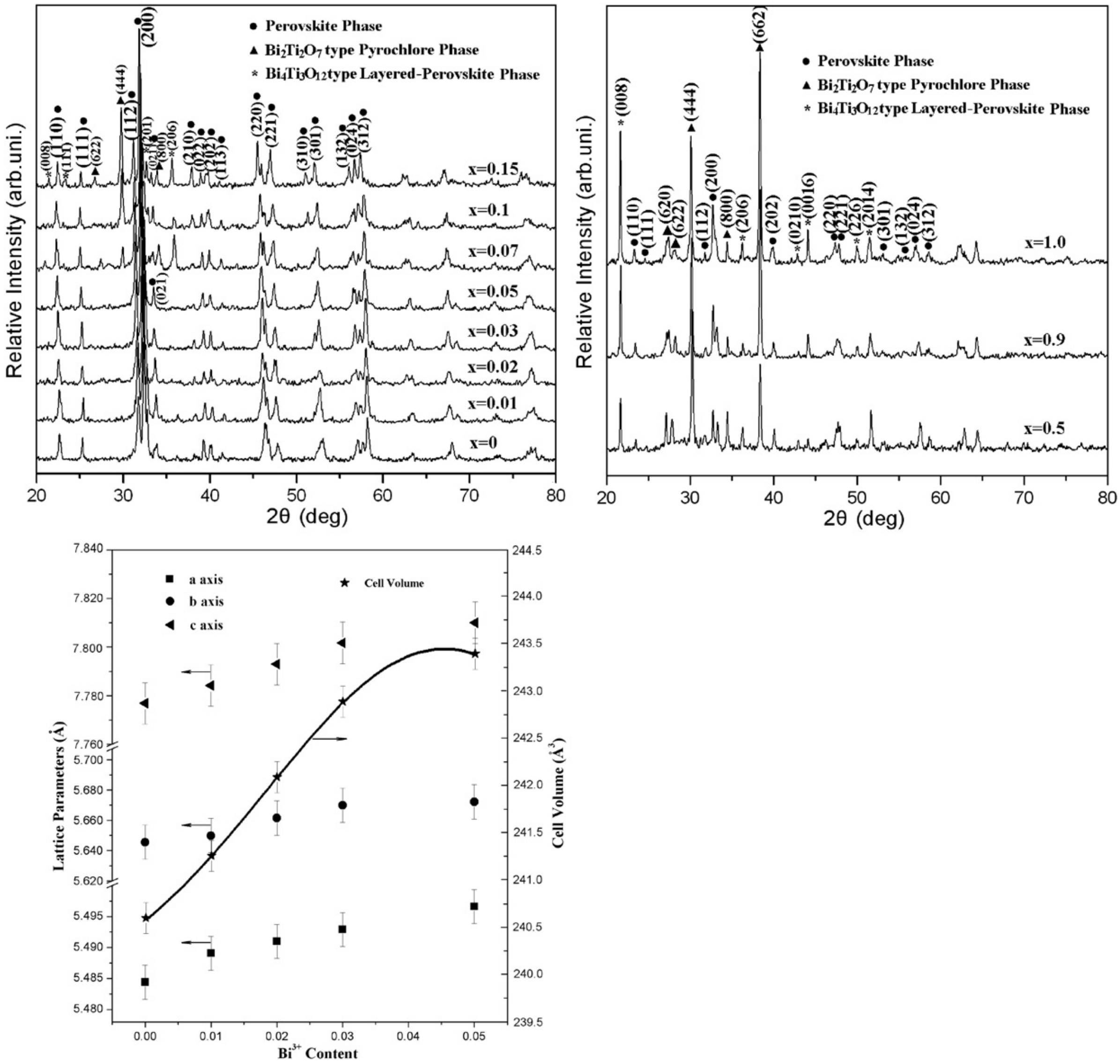

Fig. 1. XRD pattern of $(1-x)$NZT–xBZT ($0 \leq x \leq 1.0$) specimens sintered at 1300 °C for 4 h. (a) $x = 0$–0.15; (b) $x = 0.5$–1.0; (c) cell parameters for $x = 0$–0.05.

the temperature compensation mechanism in $(1-x)$NZT–xBZT ceramics.

2. Experiment procedures

2.1. Sample processing

Specimen powders composed of $Bi(Zn_{1/2}Ti_{1/2})O_3$ and $Nd(Zn_{1/2}Ti_{1/2})O_3$ were individually synthesized by a conventional solid-state reaction method. High pure raw materials of Bi_2O_3 (≥99.0%), Nd_2O_3 (≥99.99%), TiO_2 (≥99.0%) and ZnO (≥98.5%) were employed. The calcining temperatures for BZT and NZT powders were 800 °C for 3 h and 1100 °C for 4 h respectively. After calcining, BZT and NZT were weighed and mixed again according to the desired stoichiometry. After being bound with 5 wt.% PVA, the powders were pressed into 12 mm diameter disks with 1–6 mm thickness at a uniaxial pressure of 150 MPa. The final sintering process was carried out at 950–1300 °C for various time (2.5–6 h) according to different x value in a closed Al_2O_3 crucible supporting by sacrificing powders.

2.2. Characterization

The densities of the sintered pellets were determined directly by measuring their weight and the apparent volume. X-ray diffraction (XRD D8, Brucker), using graphite-monochromated CuKα (λ = 1.5406 Å) radiation, was employed to identify the phase assemblage and crystal structure of the sintered samples. The diffraction data was collected from 20° to 80° with a step size of 0.02° and a sampling time of 1 s/step. While for pure NZT sample, a step size of 0.001° and an exposition time of 8 s/step were employed for scanning the weak (1 0 1) peak between $2\theta = 18°$ and 20°. The identification of phase assemblage and its corresponding indexation were based on JCPDF cards. The lattice parameters of NBZT solid solution were calculated using Celref3.0 PC software. XRF (Shimadu XRF1800) was employed for detecting the Bi_2O_3 and ZnO evaporation from the surface of ceramics. The microstructures of the specimens were observed by a scanning electron microscope (SEM Hitachi S-4800 FE-SEM), equipped with an EDS analyzer. Raman spectra were recorded at room temperature by a Renishaw inVia Laser Confocal Raman microscope, equipped with Notch Filters and a liquid-nitrogen-cooled CCD. The 10 mW output

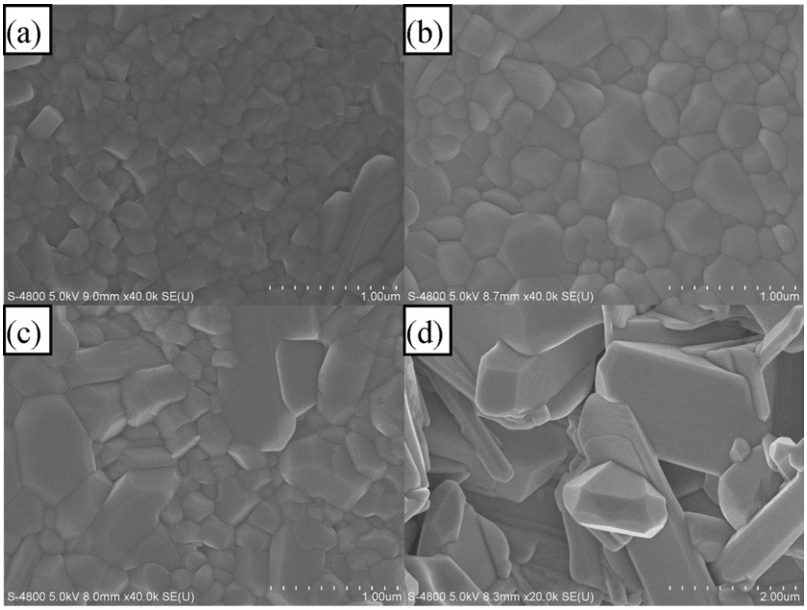

Fig. 2. SEM photographs of polished and thermally etched surface of $(1-x)$NZT–xBZT ceramics as a function of x value. (a) $x = 0.02$ sintered at 1300 °C for 2.5 h; (b)–(d) were $x = 0.02$, 0.05 and 0.07 respectively and all sintered at 1300 °C for 4 h.

of the 514.5 nm line of an Ar^+ ion laser was used as the excitation source. Dielectric properties at radio frequencies were measured by HP4192B interfaced with a refrigerator in the temperature range from 230 K to 420 K. Microwave dielectric characteristics (ε_r and Qf) were measured by means of Hakki–Coleman's resonator method using the TE_{011} mode and an ADVANTEST R3767C network analyzer (40 MHz–8 GHz). The temperature coefficients of resonant frequency were obtained by measuring the TE_{011} frequency shift in the range from room temperature to 360 K.

3. Results and discussion

3.1. Phase assemblage and microstructure analysis

Fig. 1 illustrated the X-ray diffraction patterns of $(1-x)$ NZT–x BZT ($0 \leq x \leq 1.0$) specimens. Single perovskite solid solutions formed in the composition range of $x \leq 0.05$, however, two kinds of other phases segregated from the main perovskite phase thereafter. One was the $Bi_2Ti_2O_7$-type pyrochlore phase with face-centered cubic symmetry (JCPDF 32-0118 card) and the other was $Bi_4Ti_3O_{12}$-type layered perovskite phase, also face-centered, but crystallized in orthorhombic symmetry (JCPDF 12-0213 card). Moreover, it was indicated by the following EDS that both A-site and B-site of $Bi_2Ti_2O_7$ and $Bi_4Ti_3O_{12}$ phases were partially incorporated with Nd^{3+} and Zn^{2+} respectively, thus, the crystal symmetry probably became more complicated, resulting in the preferential orientation of some crystal planes and their obviously enhanced diffraction intensity, such as the (0 0 8) diffraction peak in the $Bi_4Ti_3O_{12}$-type phase and the (6 2 2) diffraction peak in the $Bi_2Ti_2O_7$-type phase. Owning to the 6 s electronic configuration, Bi^{3+} is inclined to form a covalent chemical bond in oxide solids [16,17]. Therefore, pyrochlore phases were prone to crystallize in Bi^{3+} containing ceramics, especially at a high level of Bi^{3+} content. For example, in present $(1-x)$NZT–xBZT system, when $x \geq 0.5$, pyrochlore phase became the major phase in ceramics, as shown in Fig. 1(b).

The diffraction peaks of the main perovskite phase were indexed based on orthorhombic Pbnm (No. 62) space group, where octahedral tilting structure doubled the lattice parameter along c axis. Besides octahedral tilting, the B-site (Zn^{2+}/Ti^{4+}) 1:1 LRO structure also emerged in $x = 0$ specimen, which was indicated by a very weak (1 0 1) peak diffraction located at $2\theta = 19.84^\circ$ in XRD pattern (not shown here) as well as in Raman spectra in Fig. 4. This LRO structure slightly converted the crystal symmetry from Pbnm (No. 62) to monoclinic $P2_1/n$ (No. 14) space group at $x = 0$. A trivial systematical peak shifting toward lower 2θ angle was detected with the increase of Bi^{3+} content. The cell parameters calculated from XRD patterns for $x \leq 0.05$ illustrated an almost linear increase in cell volume, as shown in Fig. 1(c), which indicated that slightly larger Bi^{3+} (+7%) entered into the A-site substituting the 12-coordinated Nd^{3+} and forming a solid solution.

Dense and homogenous microstructure was obtained in $(1-x)$NZT–xBZT ceramics under present sintering conditions, as illustrated by SEM micrographs in Fig. 2. For the same chemical composition of $x = 0.02$, the average grain size (AGS) increased with increasing sintering time and the grain size distribution (GSD) also improved. Under the same sintering condition and an increased Bi^{3+} content, the AGS also increased but the GSD degraded. This could be due to the low melting point of Bi_2O_3 component making it beneficial for generating a eutectic liquid phase at very low temperature. This eutectic liquid phase could act as lubrication

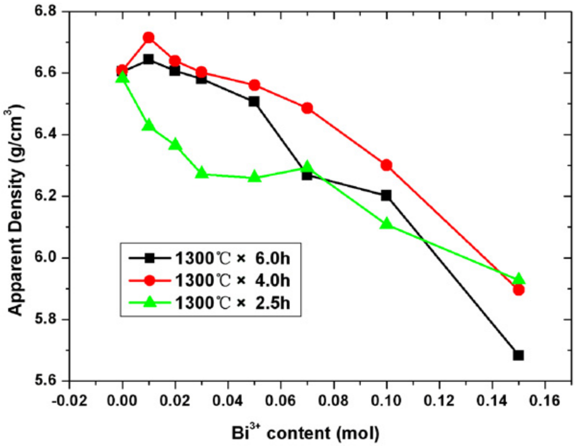

Fig. 3. Variation of apparent densities with x value in $(1-x)$NZT–xBZT ceramics sintered at 1300 °C for different time.

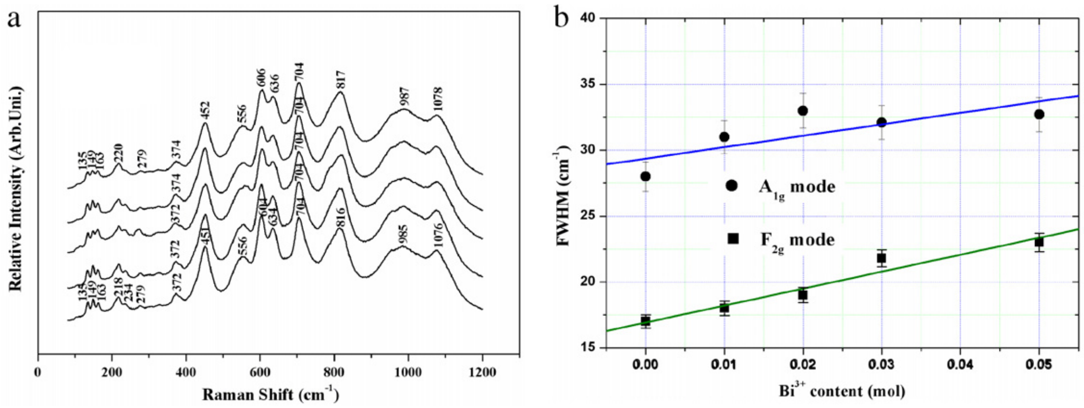

Fig. 4. (a) Raman patterns of $(1-x)$NZT–xBZT ceramics sintered at 1300 °C for 4 h as a function of x value, and (b) Raman FWHM of A_{1g} mode and F_{2g} mode in $(1-x)$NZT–xBZT ceramics.

during the sintering process, wetting solid particles and providing capillary pressure between them, resulting in a faster particle dissolving and diffusion process, and consequently, an accelerated grain growth [18]. However, as Bi^{3+} content exceeded 0.05 mol, second kind of strip-like grains separated in the microstructure and EDS analysis indicated the cation ratio of its A-site and B-site was $(M_{Bi}+M_{Nd}):(M_{Zn}+M_{Ti})\approx 4:3$. Therefore, one could presume it was the $Bi_4Ti_3O_{12}$-type layered perovskite phase, which was in agreement with the previous XRD analysis. As this phase appeared, the porosity in the bulk increased and the apparent density decreased (see Fig. 3).

Fig. 3 illustrated the apparent densities variation with x in $(1-x)$NZT–xBZT ceramics. When sintered at 1300 °C for 4 h, the apparent density firstly enhanced at $x = 0.01$, then decreased almost linearly from 6.714 g/cm^3 to 6.551 g/cm^3 as Bi^{3+} content increased from 0.01 mol to 0.05 mol. Especially when x exceeded 0.05, the apparent density reduced much faster with the increased Bi^{3+} content. This was quite unexpected. Since Bi^{3+} is heavier than Nd^{3+} and the unit cell volume expansion was negligible during Bi^{3+} substitution, the theoretical density as well as the apparent density should increase instead of decrease. The possible reason for this phenomenon could be associated with the faster grain growth as Bi^{3+} content increased, which would preclude the pore venting process during sintering and eventually increase the blocked pores in the samples [19]. Especially when $Bi_4Ti_3O_{12}$-type phase appeared after $x = 0.05$, its strip-like shape unmatched with the rounded shape of perovskite phase and thus it impeded a compact pileup in ceramics, resulting in a much faster increased porosity.

3.2. Raman spectrum analysis

Theoretically, the rock-salt 1:1 B-site ordering structure in Fm3m complex perovskites gives rise to 4 Raman–active modes of $A_{1g}+E_g+2F_{2g}$ [20]. With the symmetry further lowered by BO_6 octahedral tilting, as in $P2_1/n$ symmetry, 24 Raman-active modes will be developed as $7A_g+7B_{1g}+5B_{2g}+5B_{3g}$ [21]. However, the Raman spectra (Fig. 4(a)) in the present $Nd(Zn_{0.5}Ti_{0.5})O_3$ sample ($P2_1/n$ symmetry) only illustrated 15 Raman bands, which were located at 135 cm^{-1}, 149 cm^{-1}, 163 cm^{-1}, 218 cm^{-1}, 234 cm^{-1}, 279 cm^{-1}, 372 cm^{-1}, 451 cm^{-1}, 556 cm^{-1}, 604 cm^{-1}, 634 cm^{-1}, 704 cm^{-1}, 816 cm^{-1}, 985 cm^{-1} and 1076 cm^{-1} wavenumber respectively. The other 9 bands might either overlap with each other or be too weak to be extracted from the background. Among the exhibited 15 bands, the band at 704 cm^{-1} was assigned to the B–O symmetric stretching vibration. The bands at 451 cm^{-1} and 556–634 cm^{-1} were ascribed to the B–O torsional vibration based on the research of Levin and Hirata et al. [22,23], which included O–B–O bending or asymmetric breathing vibration of the oxygen cage. The bands in the region of 218–372 cm^{-1} were tentatively assigned to be associated with the BO_6 octahedral rotations and the band at low frequency range of 135–163 cm^{-1} was mainly related to the A-site cation environment [24].

As Bi^{3+} substituting content increased, the intensity and the full-width at half-maximum (FWHM) value of the Raman bands varied, as illustrated in Fig. 4(b). Taking 704 cm^{-1} (A_{1g}) and 372 cm^{-1} (F_{2g}) bands as examples, these two bands were well known as the “fingerprint” for the B-site ordering structure in complex perovskites

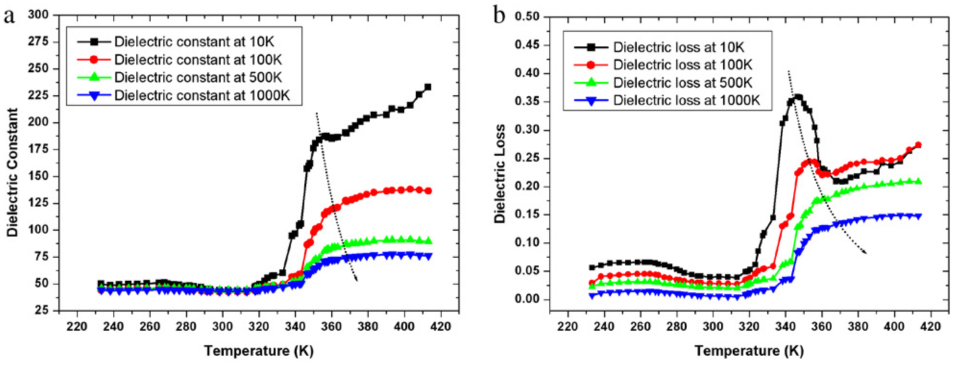

Fig. 5. Radio-frequency dielectric spectrum of $(1-x)$NZT–xBZT ($x = 0.03$) ceramics.

[25]. The F_{2g} peak, usually accompanied by an A_{1g} peak, is only sensitive to LRO structure, while the A_{1g} band is associated with both SRO (short range ordering) and LRO structure [26]. As the Bi^{3+} content increased, the FWHM of A_{1g} and F_{2g} modes increased linearly, indicating the gradual softening of the B-site ordering structure. This was clearly ascribed to the incorporation of Bi^{3+} into the $Nd(Zn_{0.5}Ti_{0.5})O_3$ perovskite, which constricted in some manner the octahedral breathing mode due to the size difference in the A-site and thus influenced the SRO degree on the B-site in NBZT complex perovskites, analogous to the research of Zheng et al. [27] in $CaTiO_3$–$Sr(Mg_{1/3}Nb_{2/3})O_3$ complex perovskites.

On the other hand, with the increase of Bi^{3+} content, the Raman bands remained almost unshifted. Bearing in mind that Bi^{3+} is larger and heavier than Nd^{3+}, we had expected a redshifting in the A-site cation related Raman bands (135–163 cm^{-1}) by employing a classical harmonic model as:

$$\omega = \sqrt{\frac{k}{m^*}}, \tag{1}$$

where ω is the Raman band frequency, k is the force constant related to the bond strength and m^* is the equivalent mass of Raman active mode. However, the stronger polarizability of Bi^{3+} (6.04 Å^3), compared with Nd^{3+} (5.01 Å^3), would lead to the increase of the bond strength between Nd/Bi–O bond, thus enhance the force constant k and counteract the effect from the increased equivalent mass, resulting in the almost unshifted Raman spectra. Moreover, the A_{1g} stretching mode was mainly determined by the strength of Ti–O and Zn–O bonds in octahedral cages. We suggested that the substitution of Bi^{3+} for Nd^{3+} only make the tilted BO_6 octahedra more regular rather than distort the octahedra themselves, thus, the B-site bond strength, or the Raman stretching mode, remained unchanged in $x \le 0.05$ range. This speculation could also be interpreted by the decreased intensity and increased FWHM value of B–O torsional vibration at 218–279 cm^{-1} and BO_6 rotational mode at 604–634 cm^{-1} wavenumber with the increase of Bi^{3+} content, which was a signal of the decreased tilting angle of BO_6 octahedral cluster in NBZT perovskites.

3.3. Dielectric properties investigation

3.3.1. Dielectric properties at radio frequencies

The temperature dependence of dielectric properties of $(1-x)$NZT–xBZT ceramics was investigated in the radio frequency range between 10^4 and 10^6 Hz. Frequency dispersion was discovered in $x = 0.03$ sample in temperature range from 230 K to 420 K. As illustrated in Fig. 5, very broad dielectric constant peaks and relatively clearer dielectric loss peaks appeared after the dispersive shoulder at 320 K and 310 K respectively. All the peaks shifted toward higher temperature and became broader with increasing frequency. As well known, in Bi-containing oxygen–octahedral system, two kinds of short-range structure imperfections usually existed, the local lattice distortions and the localized hopping charge carriers [28]. The former was developed due to the anisotropic chemical bonding characteristics of the Bi($6s^2$)–O($2p^6$) bond, which gave rise to reversible dipoles in dielectrics, while the latter stemmed from Bi_2O_3 evaporation during sintering, which was usually accompanied with Ti^{4+}/Ti^{3+} valence changing and oxygen vacancies in ceramics. This can be described in terms of Kröger–Vink notation as:

$$Bi_2O_3 \Leftrightarrow 3V_O \bullet\bullet + 2V_{Bi}'''. \tag{2}$$

In order to confirm the Bi_2O_3 evaporation in $(1-x)$NZT–xBZT ceramics, a high Bi^{3+} concentration sample, $x = 0.5$, was chosen for XRF surface analysis. As shown in Fig. 6, the Bi^{3+} concentration distribution exhibited a hyperbolic–like curve relative to the depth from surface, which clearly indicated the Bi_2O_3 diffused from the inner ceramic to the surface and evaporated to atmosphere. Thus, it was reasonable for us to assume that the Bi^{3+} evaporation or the localized hopping charge carriers exist in the $x = 0.03$ sample.

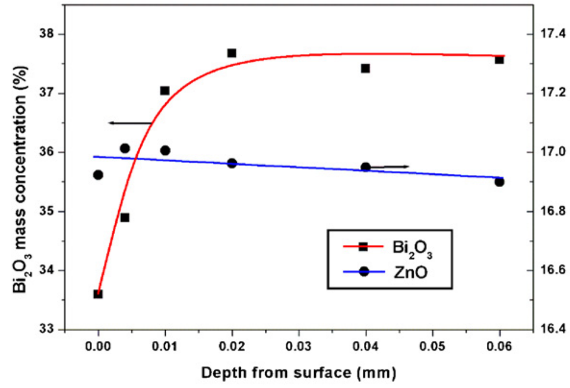

Fig. 6. Variation of Bi_2O_3 and ZnO mass concentration (%) with the depth from surface in $(1-x)$NZT–xBZT ($x = 0.5$) sample.

Since Bi^{3+} concentration was low (3 mol%), the induced reversible dipoles might distribute irregularly and independently rather than interact with each other. Therefore, the intrinsic switching frequencies of these dipoles had a wide range distribution [14]. At low frequencies, the switching frequencies of these dipoles matched the applied RF field and they predominated the contribution to the dielectric loss, as shown in the 10 K and 100 K curve in Fig. 5. However, the dipoles did not follow up the applied field as frequency increased and the contribution from hopping charge carriers became prevalent, whose typical characteristic is to rise exponentially with temperature [29]. Thus, the dielectric loss curve ascended continuously with increasing temperature thereafter.

The dielectric constant measured at radio frequencies (1 MHz) was ~48, analogous to that measured at microwave range, suggesting that there was not any frequency dispersion mechanism between 10^4–10^9 Hz at round room temperature in $(Nd_{0.97}Bi_{0.03})(Zn_{0.5}Ti_{0.5})O_3$ ceramic. Therefore, it could also be supposed that the temperature coefficient of dielectric constant (τ_ε) evaluated from the linear part (230–320 K) in Fig. 5(a) at 1 MHz be comparable with that measured at microwave frequency. Actually, τ_ε measured at 1 MHz was 25.9 ppm/K, whose magnitude featured a typical non-ferroelectric tilted perovskites behavior in vicinity of room temperature. The major contributor to dielectric constant was from the polarized phonon vibration. And the τ_ε value mea-

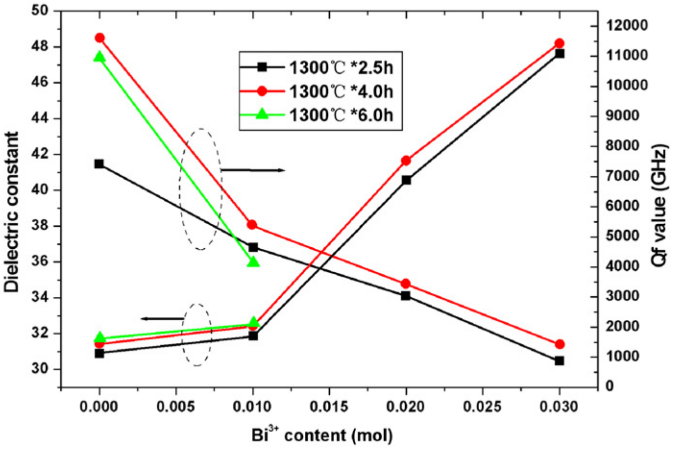

Fig. 7. Dielectric constant ε_r and Qf value of $(1-x)$NZT–xBZT ceramics sintered at 1300 °C as a function of x value.

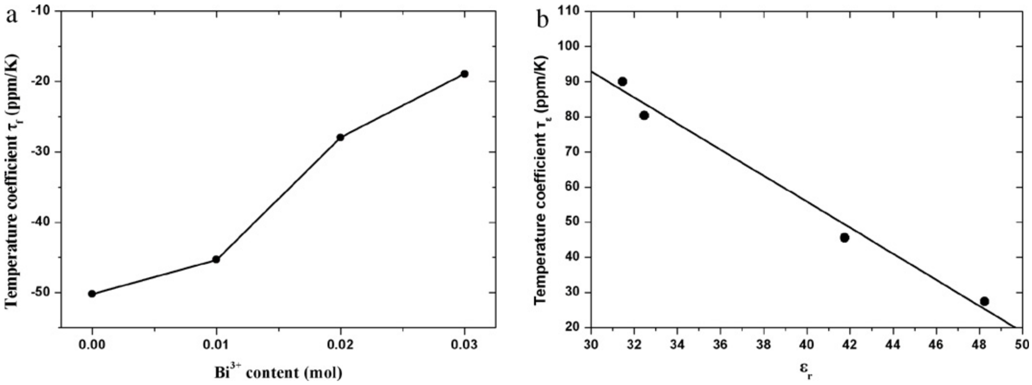

Fig. 8. (a) Temperature coefficient τ_f of $(1-x)$NZT–xBZT ceramics sintered at 1300 °C for 4 h as a function of x value, and (b) relationship between τ_ε and ε_r in $(1-x)$NZT–xBZT ceramics sintered at 1300 °C for 4 h.

sured at GHz frequency range using the $\tau_\varepsilon = -2(\tau_f + \alpha_L)$ formula was 17.8 ppm/K, where α_L is the linear thermal–expansion coefficient and was set to be 10 ppm/K for the present ceramic. Hence, it was suggested that dielectric constant and its temperature coefficient measured at RF frequencies can be a good evaluation for the values at GHz frequency range for microwave ceramics.

3.3.2. Microwave dielectric properties

The compositional dependence of the dielectric constant ε_r and *Qf* values of $(1-x)$NZT–xBZT ceramics at microwave frequencies was illustrated in Fig. 7. As x increased from 0 to 0.03, ε_r increased from 31.75 to 48.21 in a hyperbolic manner. This behavior could be rationalized by considering Claussius–Mossotti equation [30] (Eq. (3)), from which a hyperbolic function between macroscopic ε_r and ion polarizability α could be deduced as Eq. (4), assuming cell volume V is a constant (which was reasonable since V only varied 0.95% in the range of $x \le 0.03$ according to Fig. 1(c)):

$$\frac{\varepsilon_r - 1}{\varepsilon_r + 2} = \frac{4\pi\alpha}{3V}, \tag{3}$$

$$\varepsilon_r + 2 = \frac{3}{1 - k\alpha} \quad \left(k = \frac{4\pi}{3V} = \text{const}\right). \tag{4}$$

The *Qf* values descended quickly from 11,600 GHz at $x = 0$ to only 1430 GHz at $x = 0.03$. This was significant at the beginning of 1 mol% Bi^{3+} substitution, where a huge reduction of more than 50% of *Qf* value was exhibited. Many factors [31,32] were investigated for revealing the phenomenon, which included the extrinsic factors, such as order–disorder transition, impurity phases, pore density and oxygen vacancies, as well as the intrinsic factor, the unharmonic phonon vibration in microwave field. Firstly, ordering structure is widely accepted as an important factor that influences *Qf* value in complex perovskites, however, in the present perovskite, the LRO structure evolved only slightly from $x = 0$ to $x = 0.01$ (refer to Fig. 4), therefore, it seemed LRO structure was not the key reason for the sharp reduction. Secondly, a pure phase ceramic was obtained at $x = 0.01$, thus no impurity phases were responsible for the *Qf* reduction. Thirdly, the apparent density increased instead of a decrease at $x = 0.01$ (refer to Fig. 3), which indicated that the pore density in $x = 0.01$ sample also was not the reason. Fourthly, the evaporation of Bi_2O_3 during sintering would result in oxygen defects in ceramics (refer to Figs. 5 and 6), which, as widely acknowledged by many authors [33,34], has a detrimental effect on *Qf* value in dielectrics by increasing the conduction loss at microwave frequencies. Finally, the multiphonon absorption vibration in present Bi^{3+} substituted $Nd(Zn_{0.5}Ti_{0.5})O_3$ perovskite might also account for the huge *Qf* reduction. Since analogously, in Bi-substituted $La(Mg_{0.5}Ti_{0.5})O_3$ ceramics [14,35], the multiphonon absorption process caused the transverse optical phonon dampings increase by about 50% with per 1 mol% Bi^{3+} substituting. Therefore, we deduced that the significant dielectric loss mainly stemmed from two reasons, one was the oxygen vacancies arose from Bi_2O_3 evaporation and the other was the multiphonon absorption vibration caused by Bi^{3+} substitution for Nd^{3+}.

Additionally, as for the same chemical composition, the highest *Qf* values were obtained in the samples sintered for 4 h, which could be ascribed to the minimum porosities compared with the corresponding samples sintered for 2.5 h and 6 h (refer to Fig. 3). According to Kim et al. [36], porosity in dielectrics dissipates microwave energy heavily, where deteriorating effect on Q value could be described as:

$$Q = Q_0(1 - 1.5P), \tag{5}$$

where Q_0 was the intrinsic quality factor measured by infrared reflective spectrum and P represented for porosity. Therefore, 4 h was the optimum sintering time for the present ceramics.

Fig. 8(a) showed the temperature coefficient of resonant frequency (τ_f) value varied with x in $(1-x)$NZT–xBZT ceramics sintered at 1300 °C for 4 h. As illustrated, τ_f increased from −50.2 ppm/K at $x = 0$ to −18.9 ppm/K at $x = 0.03$, with the similar increasing trend as that in dielectric constant. Harrop et al. [37] and later Wise et al. [38] investigated the microscopic origins of τ_ε, related to τ_f by $\tau_\varepsilon = -2(\tau_f + \alpha_L)$ formula, by differentiating the Claussius–Mossotti equation and revealed that τ_ε was composed of three terms, A, B and C as:

$$\tau_\varepsilon = \frac{(\varepsilon - 1)(\varepsilon + 2)}{\varepsilon}(A + B + C) \approx \varepsilon(A + B + C)\Big|_{\varepsilon > 20}. \tag{6}$$

The A and B terms indicate the direct effect of volume expansion due to temperature increase, and term C represents a dependence of polarizability on temperature with a constant volume. As for most perovskite compounds, $(A + B)$ term exhibits a constant value. Therefore, the sign and magnitude of τ_ε are determined directly by magnitude of the term C. Literature on metal halides and oxides indicated that term C mainly depended on crystal structure rather than chemical composition [39]. As for present perovskite, term C could also be treated as a constant in Eq. (6) since no obvious octahedral tilting transition occurred in the solid solution range and the variation of perovskite unit cell volume could be neglected to the first approximation. Therefore, the above theoretical analysis indicated that the tuning of τ_ε in present perovskite was mainly attributed to the dilution of ε_r and the relationship between them should be linear. Our experimental data between τ_ε and ε_r manifested this theory quite well, as illustrated in Fig. 8(b). From the linear trend, the compensated τ_f value could be deduced to occur at $x = 0.05$, supposing no structure transition took place at this point. However, the too high dielectric loss in $x = 0.05$ sample unfortunately precluded the measurement of τ_f value by using the present resonant method. Hence, the nearest-to-zero τ_f value that could be obtained in $(1-x)$NZT–xBZT ceramics was -18.9 ppm/K at $x = 0.03$.

4. Conclusions

The phase assemblage, crystal structure and their relationships with dielectric properties at various frequencies in $(1-x)$NZT–xBZT $(0 \le x \le 1.0)$ ceramics were investigated. XRD diffraction results showed that a single perovskite phase was produced in the composition range of $x \le 0.05$, but the crystal lattice was distorted by both octahedral tilting and a B-site Zn^{2+}/Ti^{4+} 1:1 LRO structure. The latter lowered the crystal symmetry from orthorhombic Pbnm space group to monoclinic $P2_1/n$ space group by giving rise to a (1 0 1) superlattice diffraction at $2\theta = 19.84^{\circ}$. The more sensitive Raman spectra indicated that the LRO structure actually persisted up to $x = 0.05$, although its intensity and FWHM became gradually softened as x increased. The dielectric properties measured at RF frequency were comparable to that in GHz frequency range, however, they clearly exhibited a frequency dispersion behavior with temperature in $x = 0.03$ sample, which was suggested to be caused by two kinds of relaxor mechanisms, the reversible dipoles and the localized hopping charge carriers. The dielectric constant measured at GHz frequency range gradually increased from 31.75 to 48.21 as x varied from 0 to 0.03, meanwhile, the *Qf* value decreased sharply and monotonously from 11600 GHz to 1430 GHz. The temperature coefficient of resonant frequency could be effectively tailored by Bi^{3+} substitution. It increased from -50.2 ppm/K to -18.9 ppm/K as Bi^{3+} content increased from 0 to 3 mol%. The nearly compensated τ_f value in 0.97NZT–0.03BZT ceramic was mainly attributed to the dilution of dielectric constant according to the structure-related thermal parameter analysis.

Acknowledgements

The first author thanks Dr. Yu Wang from Hong Kong Polytechnic University for the critical and constructive discussion. Great appreciation is given to the National Science Foundation of China (No. 50371056, No. 61076049) and to the State Key Laboratory of New Ceramics & Fine Processing, Tsinghua University (No. KF0706) for their financial support. Prof. H.S. Gu also acknowledges the financial support of the International Science and Technology Cooperation Project granted 2009DFB50470.

References

[1] M.Z. Hu, H.S. Gu, X.C. Chu, J. Qian, Z.G. Xia, J. Appl. Phys. 455 (2008) 475–485.
[2] M.P. Seabra, A.N. Salak, V.M. Ferreira, J.L. Ribeiro, L.G. Vieira, J. Eur. Ceram. Soc. 24 (2004) 2995–3002.
[3] D.L. Cairns, I.M. Reaney, H. Zheng, D. Iddles, T. Price, J. Eur. Ceram. Soc. 25 (2005) 433–439.
[4] C.H. Hsu, Y.S. Chang, J. Alloys Compd. 479 (2009) 714–718.
[5] Y.B. Chen, J. Alloys Compd. (2010), doi:10.1016/j.jallcom.2010.09.170.
[6] S. Kucheiko, H.J. Kim, D.H. Yeo, H.J. Jung, Jpn. J. Appl. Phys. 35 (1996) 668–672.
[7] C.H. Hsu, J. Alloys Compd. 464 (2008) 412–417.
[8] A.N. Salak, O. Prokhnenko, V.M. Ferreira, J. Phys.: Condens. Matter 20 (2008) 1–9, 085210.
[9] I. Levin, J.Y. Chan, J.E. Maslar, T.A. Vanderah, J. Appl. Phys. 90 (2001) 904–914.
[10] Y.B. Chen, J. Alloys Compd. 478 (2009) 781–784.
[11] C.L. Pan, C.H. Shen, P.C. Chen, T.C. Tan, J. Alloys Compd. 503 (2010) 365–369.
[12] M. Spreitzer, J. König, B. Jancar, D. Suvorov, IEEE Trans. Ultrason. Ferroelectr. Freq. Control 54 (2007) 2617–2622.
[13] C.N. Juan, T.L. Michael, A.R. Clive, K. Stanislav, Appl. Phys. Lett. 81 (2002) 4404–4406.
[14] A.N. Salak, V.M. Rerreira, J.L. Ribeiro, L.G. Vieira, R.C. Pullar, N.M. Alford, J. Appl. Phys. 104 (2008) 014105.
[15] C.L. Huang, W.R. Yang, Mater. Lett. 63 (2009) 103–105.
[16] Y. Inaguma, A. Miyaguchi, T. Katsumata, Mater. Res. Soc. Symp. Proc. 755 (2003) 471–476.
[17] C.A. Randall, R. Eitel, B. Jones, T.R. Shrout, D.I. Woodward, I.M. Reaney, J. Appl. Phys. 95 (2004) 3633–3639.
[18] R.M. Germen, Liquid Phase Sintering, Plenum Publishing, New York, 1985, p. 239.
[19] V.A. Izhevskyi, A.H.A. Bressiani, J.C. Bressiani, J. Am. Ceram. Soc. 88 (2005) 1115–1121.
[20] R. Tao, I.G. Siny, R.S. Katiyar, R. Guo, A.S. Bhalla, J. Raman Spectrosc. 27 (1996) 873–877.
[21] M. Zaghrioui, A. Bulou, P. Lacorre, P. Laffez, Phys. Rev. B 64 (2001) 081102.
[22] T. Hirata, K. Ishioka, M. Kitajima, J. Solid State Chem. 124 (1996) 353–359.
[23] I. Levin, J.Y. Chan, R.G. Geyer, J.E. Maslar, T.A. Vanerah, J. Solid State Chem. 156 (2001) 122–134.
[24] P.V. Bijumon, M.T. Sebastian, A. Dias, R.L. Moreira, P. Mohanan, J. Appl. Phys. 97 (1–9) (2005) 104108.
[25] E. Husson, L. Abello, A. Morell, Mater. Res. Bull. 25 (1990) 539–545.
[26] U. Bismayer, V. Devarajan, P. Groves, J. Phys.: Condens. Matter 1 (1989) 6977–6981.
[27] H. Zheng, H. Bagshaw, G.D.C. Gyorgyfalva, I.M. Reaney, R. Ubic, J. Yarwood, J. Appl. Phys. 94 (2003) 2948–2956.
[28] O. Bidault, M. Maglione, M. Actis, M. Kchikech, B. Salce, Phys. Rev. B 52 (1995) 4191–4197.
[29] C. León, A. Riveraa, A. Várezc, J. Sanzb, J. Santamariaa, C.T. Moynihand, K.L. Ngaie, J. Non-Cryst. Solids 305 (2002) 88–95.
[30] R.D. Shannon, J. Appl. Phys. 73 (1993) 348–366.
[31] M. Valant, D. Suvorov, C.J. Rawn, Jpn. J. Appl. Phys. 38 (1999) 2820–2826.
[32] D.M. Iddle, A.J. Bell, A.J. Moulson, J. Mater. Sci. 27 (1992) 6303–6310.
[33] A.N. Salak, V.M. Ferreira, J. Eur. Ceram. Soc. 27 (2007) 2887–2891.
[34] R.C. Pullar, S.J. Penn, X. Wang, I.M. Reaney, N.M. Alford, J. Eur. Ceram. Soc. 29 (2009) 419–424.
[35] F. Azough, R. Freer, C.L. Wang, G.W. Lorimer, J. Mater. Sci. 31 (1996) 2539–2549.
[36] E.S. Kim, H.S. Park, K.H. Yoon, Mater. Chem. Phys. 79 (2003) 213–217.
[37] A.G. Cockbain, P.J. Harrop, J. Phys. D: Appl. Phys. 1 (1968) 1109–1115.
[38] P.L. Wise, I.M. Reaney, W.E. Lee, D.M. Iddles, D.S. Cannell, T.J. Price, J. Mater. Res. 17 (2002) 2033–2040.
[39] A.J. Bosman, E.E. Havinga, Phys. Rev. 129 (1963) 1593–1604.